Optimal properties of porous materials and non-wetting liquids for heat of intrusion-extrusion maximization

ELECTRO-INTRUSION PROJECT

HORIZON 2020 | FETPROACT-EIC-07-2020
FET Proactive: Emerging paradigms and communities

GRANT AGREEMENT No. 101017858

Deliverable No.	D3.1	
Deliverable Title	Optimal properties of porous materials and non-wetting liquids for heat of intrusion-extrusion maximization	
Due Date	31.12.2024	
Deliverable Type	Report	
Dissemination level	Public	
Written by	Alexander Lowe, Simone Meloni, Emre Arkan, Miroslaw Chorazewski, Yaroslav Grosu	09.07.2024
Approved by	General Assembly	12.12.2024
Status	Final	15.12.2024

European Innovation Council
Funded by the European Union

REVISION HISTORY

Version	Date	Author	Partner	Changes
0	09.07.2024	Alexander Lowe	USK	1st version

TABLE OF CONTENTS

LIST OF TABLES AND FIGURES

LIST OF ABBREVIATIONS

Acronym / Short name	Meaning
EXT	extrusion
H	Enthalpy
INT	intrusion
MD	Molecular Dynamics
MOF	Metal–organic framework
Q	Heat
P	Pressure
PEI	Polyethylenimine
RMD	Restrained molecular dynamics
ST	Scanning Transitiometry
T	Temperature
U	Internal energy
V	Volume
VMD	Visual Molecular Dynamics
WC	Waters Carbon
ZIF	zeolitic imidazolate framework
Tert	tert-butanol

PROJECT ABSTRACT

– Simultaneous transformation of ambient heat and undesired vibrations into electricity via nanotriboelectrification during non-wetting liquid intrusion-extrusion into-from nanopores –

Greenhouse gas emissions, pollution and rational energy use are civilization-scale challenges which need to be resolved urgently, in particular by the conversion of abundant waste heat and undesired vibrations into useful electricity. However, the low efficiency of existing conversion methods does not provide an attractive solution.

Electro-Intrusion project proposes a new and highly efficient method and apparatuses for the simultaneous transformation of mechanical and thermal energies into electricity by using zero-emission nanotriboelectrification during non-wetting liquid intrusion-extrusion into-from nanoporous solids.

To tackle these phenomena, Electro-Intrusion project brings together a consortium of multidisciplinary teams specializing in physics, chemistry, material science and engineering to address the project by the state-of-the-art methods of molecular dynamic simulations, high-pressure calorimetry and dielectric spectroscopy, materials synthesis and characterization, and prototype development. The FET-PROACTIVE call is a key solution to bring this early-stage multidisciplinary concept to higher TRLs, fill in the large knowledge gaps in the solid-liquid contact electrification and heat generation during intrusion-extrusion as well as enable its full impact on EU innovation leadership, competitive market and energy sector security.

The proposed method can be used for energy scavenging within a wide range of technologies, where vibrations and heat are available in excess (train, aviation, domestic devices, drilling, etc.). In particular, using European Environment Agency data, this project estimates that the use of the proposed approach only within the automobile sector can reduce the overall EU electricity consumption by 1-4% in 2050. With this regard, the final stage of the project implies regenerative shock-absorber development and field-testing for a drastic maximization of the maximum range of hybrid / electric vehicles.

Electro-Intrusion project is scheduled to run from January 1st, 2021 to December 31st, 2024, for a total duration of 48 months and has received funding from the European Union's H2020 research and innovation programme under grant agreement No. 101017858. A full list of partners and funding can be found at: https://cordis.europa.eu/project/id/101017858/es. It has been extended to run till 31st of December 2025.

1 EXECUTIVE SUMMARY

This deliverable describes the results of *Work Package 3 – Understanding heat of intrusion-extrusion*, leaded by USK. Given that thermal effects of the intrusion-extrusion play significant role in the overall energy balance of this process, understanding and controlling them is of high practical and fundamental importance.

The challenge of this task is related to the nano- and subnanoscale of the phenomena, that does not allow complete reliance on the available macroscopic understanding for the thermal effects of wetting-dewetting.

The deliverable describes several novel strategies investigated to successfully tune the heat of intrusion-extrusion, as well as effect of temperature, pore size and topology on these values. It combines the materials developed and characterized by CICe, calorimetric experiments performed by USK and simulations done by UniFe.

Overall, the deliverable describes the progress in understanding heat of intrusion-extrusion for the benefit of optimal functioning of regenerative intrusion-extrusion shock absorber developed as the target application of Electro-intrusion.

2 INTRODUCTION

In this section the results of Work package 3 are presented, divided into sections highlighting the challenges and insights gained for the goal titled *optimal properties of porous materials and non-wetting liquids for heat of intrusion-extrusion maximization*. To meet this goal, a combination of high-pressure scanning calorimetry measurements and molecular dynamic simulations were used in tandem to collect and evaluate thermodynamic data under a broad range of conditions.

3 INVESTIGATED SYSTEMS

Two different solid systems were studied: the nanoporous metal-organic framework ZIF-8 and mesoporous silicas, which are further subdivided into two types with different grafting moieties (hydrocarbon (WC-8) and analogous perfluorocarbon chains). The intruding liquids in these systems were water and aqueous solutions. With later, the idea was to utilise simple properties of solutions, such as surface entropy and heat of dilution properties of aqueous solutions to alter the intrusion-extrusion characteristics. These solutions were the ionic salt KBr and the alcohol tert-butanol [1]. The last solid system is a comparison of two different mesoporous silicas with chemically-distinct grafting. One being hydrocarbon based and the other being a perfluorinated carbon analogue. The thermal effects were studied at various temperatures and solution concentrations.

Finally, heavy water or deuterium oxide was used since it demonstrated greater degree of electrification as reported in Deliverable 2.1.

Over 200 calorimetric experiments and over 20 million core hours of simulations were conducted. This equated over 600 days, shared between both partners, to study these conditions, impacted significantly by the limited literature data [2-5] combined with our original data from this project. This combination significantly improved our understanding of the heat of liquid intrusion-extrusion into-from porous systems and resulted in two publications of the Electro-intrusion consortium [1,6].

From these experiments and simulations, we have identified which are the most significant parameters affecting the heat of intrusion-extrusion cycles. The concentrations of solutes that can be used to modify the heat output and additionally affect the chemical stability of the solid materials by altering the experimental conditions (*e.g.* pH). The effect of the presence or absence of gases, which can penetrate into the pores was also explored. The heat effects from these dilute pore-intruding solutes are small enough to have no visible effect on the heat of intrusion/extrusion [6]. The effect of the particle size of ZIF-8 (from microscopic to nanoscopic) was also studied to see how it would affect the thermal output during the intrusion-extrusion cycle. Finally, the effect of surface grafting on the heat of intrusion-extrusion of mesoporous silicas was investigated by replacing grafted hydrocarbons with perfluorinated analogues.

4 INVESTIGATIVE METHOD: MEASURING THE HEAT OF INTRUSION-EXTRUSION

Scanning Transitiometry (ST) was a suitable instrumental method for determining the change of state variables whilst simultaneously measuring heat exchange during a quasi-equilibrium process. This approach enabled both accurate and precise measurements of the response of the hydrophobic porous materials when the non-wetting liquid was intruded-extruded into-from it. The temperature was kept constant while pressure was changing in a scanning manner, recording volume and heat variations.

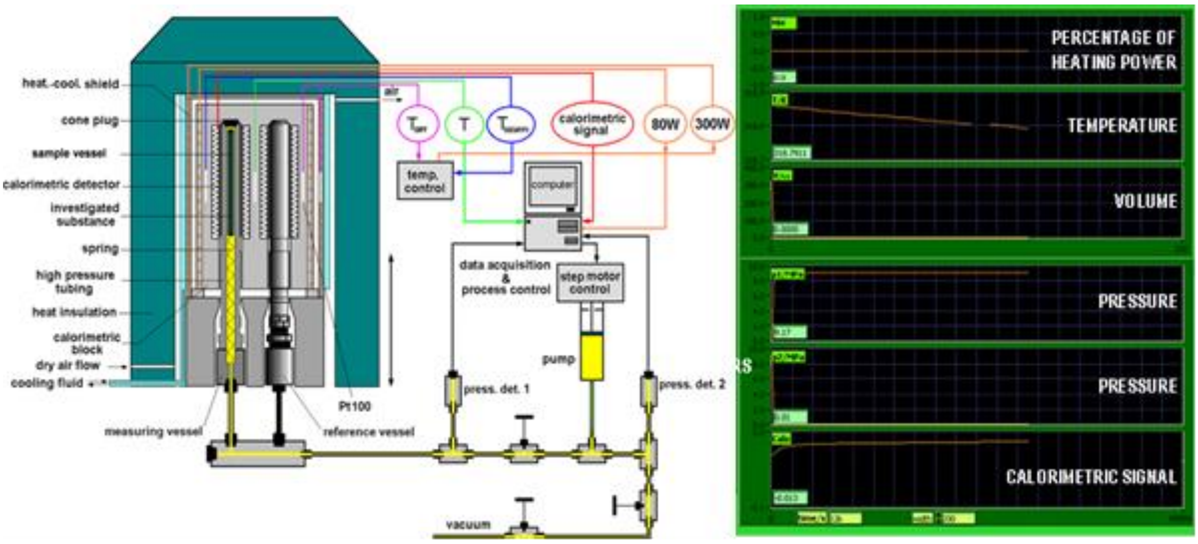

Figure 1.- Scheme of a scanning Transitiometer on the left and the recording of variables on the right.

To ensure experimental consistency, both measuring and reference cells of the transitiometer were filled with the same non-wetting liquid. The increase in pressure at a constant rate for both cells allowed the measurement of the heat flux associated with the intrusion-extrusion of non-wetting liquids. For the chosen hydrophobic porous materials and non-wetting liquids, pressure and volume are crucial factors since they permit the measurement of thermodynamic properties of the solid-liquid system under isothermal conditions.

A large number of experiments were conducted to determine the various effects regarding the heat of intrusion into ZIF-8, ZIF-8 nanoparticles, and grafted silica provided by the CICe as part of WP2.

5 {ZIF-8 + water} Systems

Our calorimetric results for {ZIF-8 + water} system differed significantly from those reported [2]. In the original manuscript, intrusion was endothermic and extrusion exothermic, while we recorded the opposite [1,6].

In this series of experiments, we compared our results to the literature [2] to understand what changes could be made to the intruding liquids. Initially, small intruding solutes were tested to observe the effect on the evolution of heat by intrusion and extrusion with respect to temperature. These ZIF-8 experiments were conducted under various conditions: the presence and absence of atmospheric gases, dilute concentrations of carbonic acid (prepared by dissolving dry ice in water), and ammonia (NH_3), which lead to small changes in the pH of the solution. Acidic solutions dissolved the ZIF-8 solid during the experiment, while basic solutions increased the number of cycles to which ZIF-8 may be subjected. In both cases, the heat of intrusion values did not change; they remained exothermic in contrast to the literature values [2], which reported endothermic behaviour upon intrusion. The inclusion of atmospheric gases had no effect on the heats of intrusion and extrusion, but did affect the specific intrusion volume ($cm^3.g^{-1}$). These results were presented in a recently published article in 2024 by Lowe *et al* [6]. Dilute concentrations of solutes, be they gases from the atmosphere or artificially introduced substances, were not able to affect the heat of intrusion.

The effect of temperature was then evaluated. The new heat of intrusion results from all experiments are presented in Figure 2 (black circles) and discussed below.

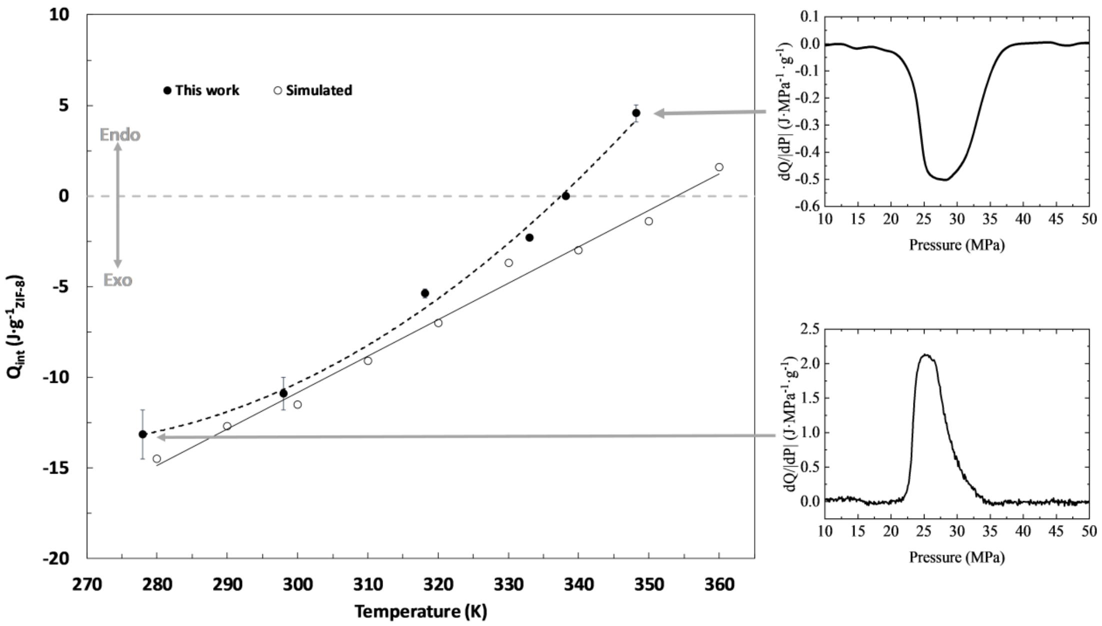

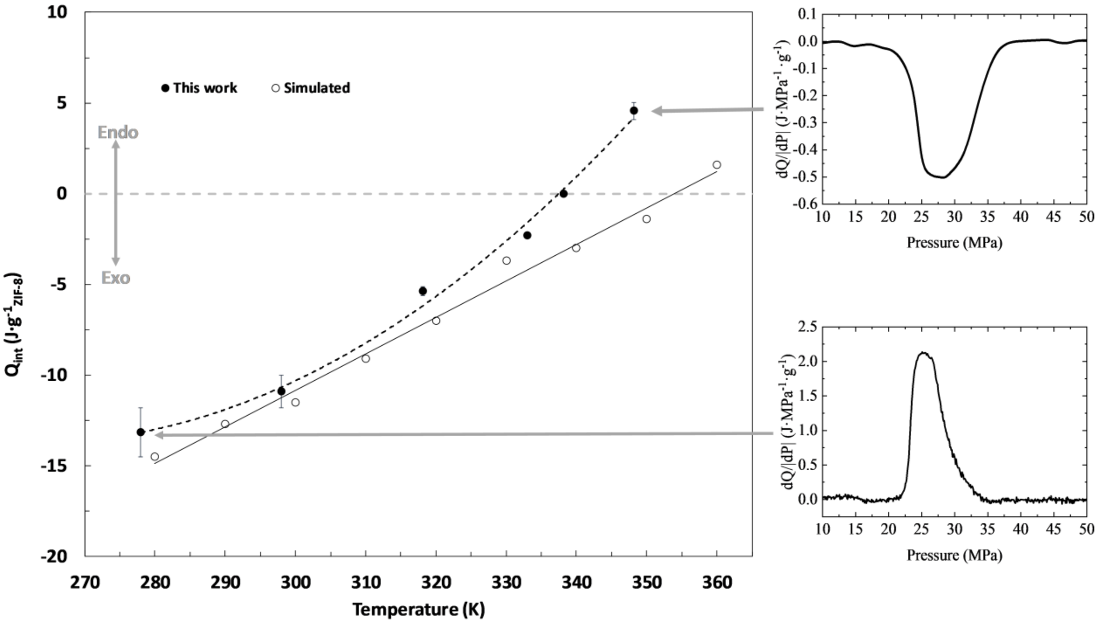

Figure 2.- Intrusion heat for {ZIF-8 + water} system. Simulations give a qualitative agreement. The results include all heat of intrusion measurements from NH3 solution at pH 10.3 and the presence/absence of atmospheric gases. The insets include the heat of intrusion (exothermic) at 278 K and (endothermic) 348 K with atmospheric gases. Taken from Lowe *et al* 2024 [6]

5.1 Strategies for making intrusion endothermic:

5.1.1 Effect of the temperature on the thermal effects

At low temperature (278 K), the largest specific heat value was recorded: an exothermic heat of intrusion of approximately -13 J·g^{-1} for ZIF-8. The change in heat with rising temperature describes a parabolic curve, with the absolute heat decreasing until it reaches a transition point at 333 K where intrusion is athermic. At 348 K the heat of intrusion is endothermic, with a value of approximately 4 J·g^{-1}. Using MD simulations, it is possible to understand the origin of this temperature dependence. It was ascribed to the difference in the heat capacity of the ZIF-8 and water system when it is in the intruded or extruded state.

The Kelvin-Laplace equation $\frac{dQ}{dA} = T\ \frac{d[\gamma(T)\cos\theta(T)]}{dT}$ [7] relates the intrusion heat per unit area of a material to the surface tension of the liquid γ, the contact angle with the solids θ, and their temperature dependence. This equation states that for two materials with the same characteristics, the one presenting a larger specific surface area (A) is best suited for thermal energy harvesting.

Restrained molecular dynamics (RMD) simulations [8, 9] were used to study the filling process of a ZIF-8 slab. This technique allowed the computation of the free energy and internal energy (or enthalpy) along the filling process. By simple arithmetic ($T\Delta S = \Delta Q = \Delta H - \Delta F$), the heat of intrusion under thermodynamic equilibrium was obtained. The heat of intrusion could also be obtained from the variation of the internal energy and the mechanical work of pressure during intrusion: $T\Delta S = \Delta Q = \Delta U + P\Delta V$. The heat of intrusion of water in a ZIF-8 slab obtained with these two methods is shown in Figure 3. The heat of intrusion calculated at complete filling (100 % filling, minimum of the free energy *vs.* the number of water molecules in the slab before over pressurization starts) was between -70 and -90 J·g^{-1}. While the directionality of the heat of intrusion was consistent with experimental results obtained within the project, the absolute value was 7-9 times greater.

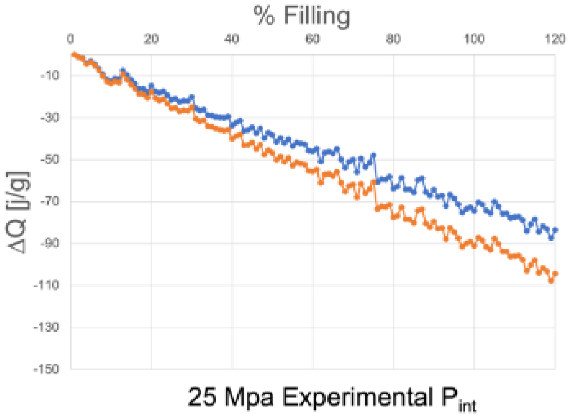

Figure 3.- Heat of intrusion filling a ZIF-8 slab. For this computational sample, the process was found to be exothermic, both by free energy calculations (blue) and the relation between internal energy and mechanical work (orange).

To investigate further, analogous calculations were performed on the wetting/drying of a single cage of the ZIF-8 slab - Figure 4. The rationale for this validation test was that the (single) filling order parameter was unlikely to be a good collective variable for the intrusion process of the entire slab. Despite combining replica exchange with RMD, the sampling of the given ensemble could have been biased and the estimate of the heat of intrusion could have been affected by a sizable error. This error should be absent or minor for the simpler case of the filling of a single cage.

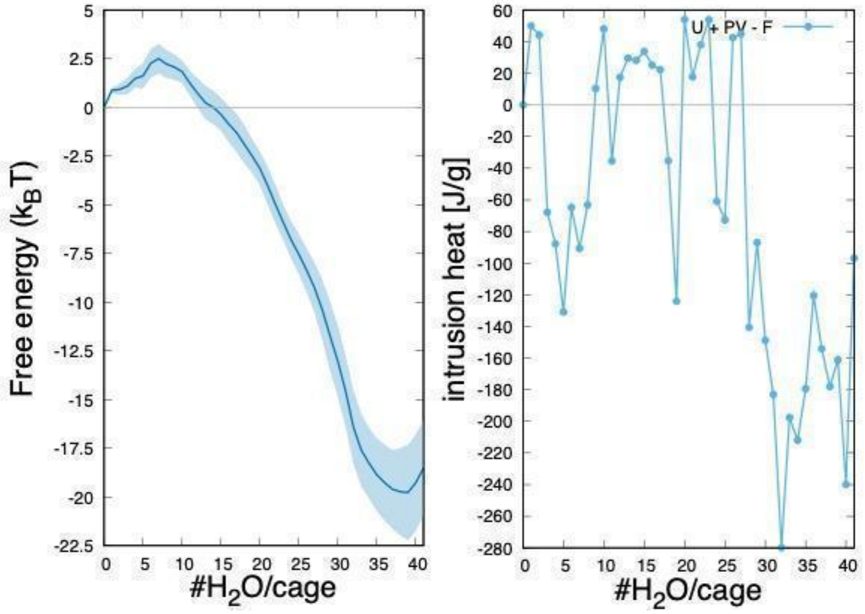

Figure 4.- Filling of a single ZIF-8 cage (left). Free energy of intrusion (right). The corresponding heat of intrusion. There were large fluctuations of the heat of intrusion observed. This agrees with the results for the intrusion of the entire slab, the intrusion of a single cage was also exothermic. There was a sudden drop of heat of intrusion around 25-30 water molecules in the ZIF-8 cavity.

These results presented another challenge: the variation of the internal energy (U)/enthalpy (H) along intrusion, necessary to compute the heat of the process, fluctuated significantly. The issue was that all the atoms of the sample, including the larger number of water molecules outside the porous system, were contributing to the internal energy/enthalpy, and their contribution to the normal fluctuation of U/H was of the same order of magnitude or larger than the variation associated with intrusion. To limit this issue, the energy distribution at each level of intrusion was calculated and fitted with Gaussian functions, from which a more reliable value of the internal energy (the centre of the Gaussian function) was extracted. This allowed the estimation of the heat of intrusion versus the number of water molecules in the cavity reported in Figure 5.

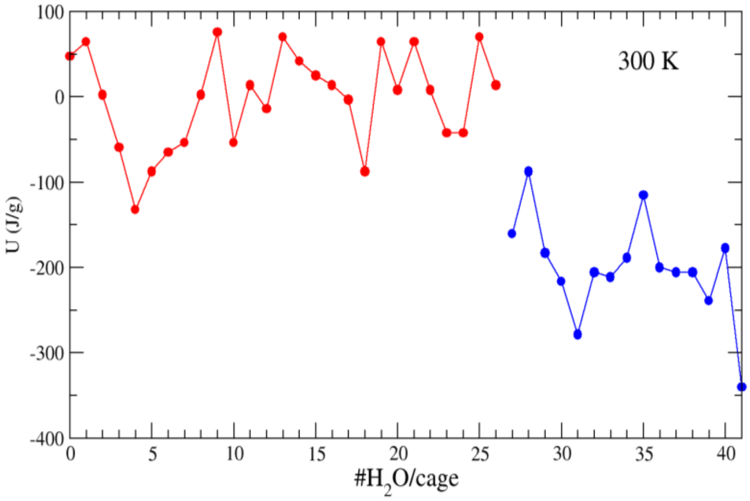

Figure 5.- Values of internal energy extracted from the Gaussian distributions of energy at each level of filling. The results are clearer than in Figure 4 but the conclusion is the same: intrusion is exothermic, with a discontinuous energy change at ~25 water molecules in the cavity.

With this approach, we estimate a heat of intrusion of ~ -190/200 J·g^{-1}, in line with the value estimated for the intrusion of water in the entire slab, and much larger than the experimental value.

To complete this, the heat of intrusion was also estimated by the Kelvin-Laplace equation. The validity of the equation at the nanoscale, when the solid/liquid interface cannot be approximated by the sharp interface model, is questionable since concepts such as surface tension and contact angle break down. The advantage of this approach was that it allowed for the derivation of simple tuning principles that qualitatively informed the efforts of the experimental partners. The Kelvin-Laplace equation requires the value of the contact angle of the internal ZIF-8 walls and its dependence on the temperature. As the cavities of ZIF-8 are too small to allow the formation of a liquid droplet, this was not possible neither in experiments nor in simulations. The energetic meaning of the Young contact angle was calculable: $cos\,\theta\; = \frac{\gamma_{SG}-\gamma_{SL}}{\gamma}$, where γ_{SG} and γ_{SL} are the solid-gas and solid-liquid surface tensions, respectively. The interfacial contact angle θ can also be computed via the Young-Duprè equation $cos\,\theta\; = \frac{W_{SL}}{\gamma-1}$, where W_{SL} is the work of adhesion of water to the ZIF-8 cavity, a quantity that can be computed via an approach derived some years ago by theoretical partners of this team [10]. In Figure 6, the trend of the contact angle with temperature is shown as derived from the Young-Duprè equation, with work of adhesion obtained from simulations.

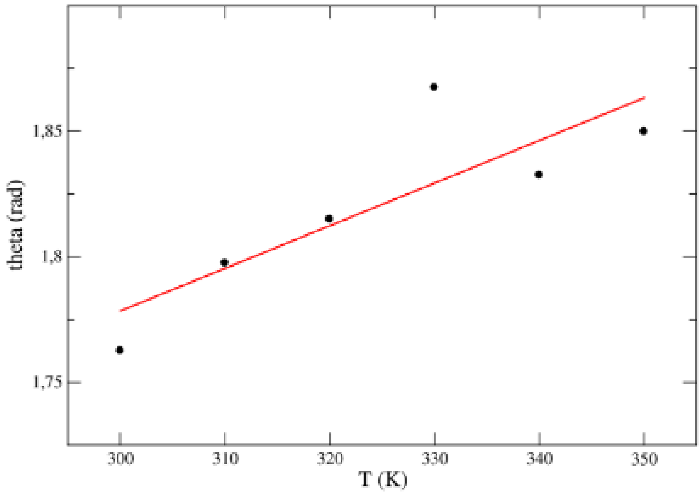

Figure 6.- ZIF-8 contact angle of the internal surface. The red line represents the linear fitting.

The heat of the intrusion obtained via this approach (Figure 7) is in semi-quantitative agreement with the atomistic, free-energetic method discussed in the previous paragraph.

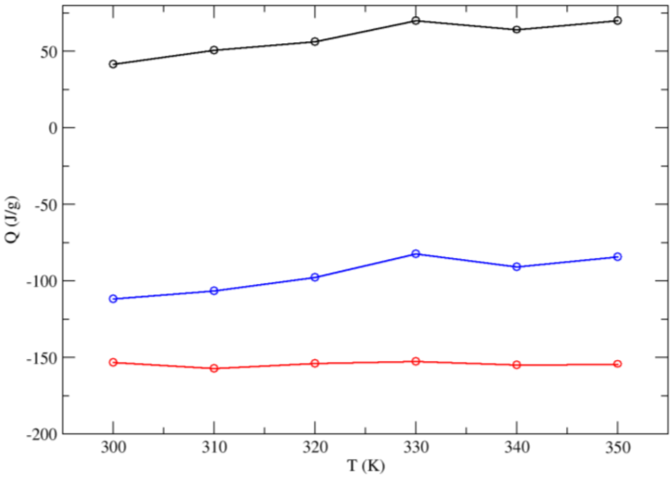

Figure 7.- Intrusion heat (blue line) via Kelvin-Laplace law as a function of temperature. The black and red lines are the contribution to the intrusion heat arising from the derivative of the surface tension and contact angle with respect to T, respectively. Note that the first term gives an endothermic contribution, while the second gives an exothermic one, with this second contribution dominating over the first one.

This large exothermic intrusion was the result of the sum of an endothermic term associated with the change in surface tension of water with temperature and an exothermic change in contact angle with T. In particular, $d\gamma/dT$ was obtained from the literature for the TIP4P/2005 water model used in these calculations and the change in the contact angle with the temperature was obtained from these calculations via the Young-Duprè equation. The trend of the internal contact angle obtained from these simulations was consistent with the change of the external contact angle of ZIF-8 measured by the experimental partners. This suggests that the very large, overestimated value of the exothermic heat of intrusion is not the result of some error in the computational campaign or a consequence of poor force fields for the simulations at hand. What is still left to be investigated is the possibility of some simultaneous endothermic process occurring during intrusion that is neglected in the simulations. Some possibilities are already being investigated, which we omit from this report because this research is still too preliminary.

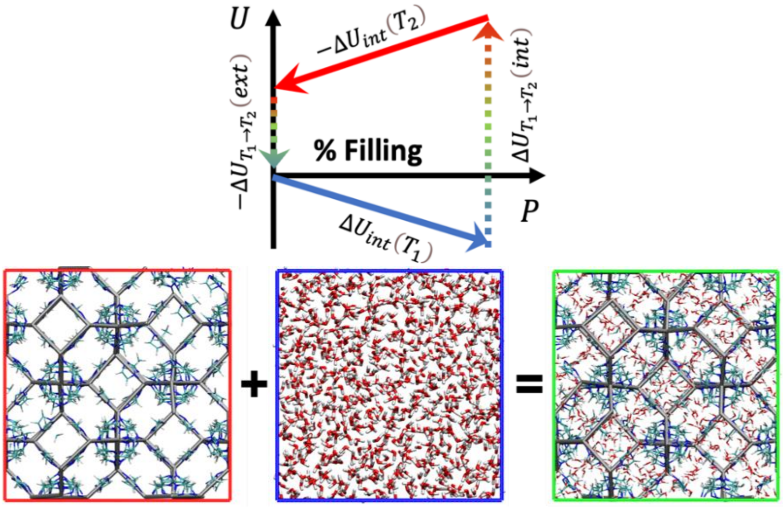

Figure 8.- Thermodynamic cycle used to determine the temperature dependence of the heat of intrusion. The first step consists of the isothermal filling of ZIF-8 at T1. Then, the filled system was warmed up from T1 to T2. At T2, the system was extruded. Finally, the extruded system was cooled down back from T2 to T1, reaching the initial state. Underneath, a visualisation of the empty ZIF-8, bulk water and fully intruded ZIF-8.

To make intrusion endothermic and maximise the effect, the temperature at which the process takes place was modified. Experimentally, it was observed that while intrusion in ZIF-8 was exothermic at lower temperatures, it became endothermic at higher values with a positive dQ/dT. To explain this trend, we follow the thermodynamic cycle shown in Figure 8, which consists of four branches: an isothermal intrusion at temperature T_1 and an isothermal extrusion branch at T_2, an isobaric heating and an isobaric cooling between T_1 and T_2 for the intruded and extruded system. The four branches were assumed to be under quasi-equilibrium conditions, which imply reversibility. In these simulations, we make two assumptions: $P_{int}(T_1) \sim P_{int}(T_2)$ and $\Delta V_{int}(T_1) \sim \Delta V_{int}(T_2)$, which are reasonable for small changes in T. Within this approximation, the following equations were derived:

$$\frac{q_{int}(T_1) - q_{int}(T_2)}{m^{ZIF-8}} = \frac{m^{ZIF-8} + m^{H_2O}}{m^{ZIF-8}}$$

$$\left[\frac{m^{ZIF-8}}{m^{ZIF-8} + m^{H_2O}} C_p^{ZIF-8}(T_2) + \frac{m^{H_2O}}{m^{ZIF-8} + m^{H_2O}} C_p^{H_2O}(T_2) - C_p^{ZIF-8+H_2O}(T_1)\right]$$

$$= \frac{m^{ZIF-8}+m^{H_2O}}{m^{ZIF-8}} \Delta \underline{C}_p \Delta T \qquad (1.2.3.2.1)$$

where $q_{int}(T)$ is the heat of intrusion at temperature T, C_p^{ZIF-8}, $C_p^{H_2O}$ and $C_p^{ZIF-8+H_2O}$ are the heat capacities of ZIF-8, bulk water and intruded ZIF-8, respectively. m^{ZIF-8} and m^{H_2O} are the masses of ZIF-8 and of the intruded liquid. The change of the heat of intrusion with T, $q_{int}(T_1) - q_{int}(T_2)$, is proportional to the (mass weighted) change in heat capacities of the involved species in the extruded and intruded states. The final mathematical relation connects the change in heat of intrusion to the (mass weighted) change in heat capacity between the extruded and intruded states to the ratio of the mass of the intruded state over the mass of the porous medium. At the limit of $\Delta T \to 0$, Eq. (1.2.3.2.1) gives a relation for the derivative of the heat of intrusion:

$$\frac{dQ}{dT} = \frac{m^{ZIF-8}+m^{H_2O}}{m^{ZIF-8}} \Delta \underline{C}_p \qquad (1.2.3.2.2)$$

The heat capacity of the three systems necessary to compute $\Delta \underline{C}_p$ can be obtained from fluctuations of their enthalpy H in simulations of the corresponding bulk triperiodic system ("statistical mechanic" approach - [11], see Figure 8): $C_P = \frac{\Delta H^2}{k_B T^2}$, with k_B the Boltzmann constant. In Figure 2, we reported experimental heat of intrusion between $278\,K$ to $343\,K$ together with theoretical predictions. Based on the estimated change of (mass averaged) heat capacity, simulations predict a positive change of heat of intrusion of 19 $1\,J \cdot g_{ZIF-8}^{-1}$ over a $70\,K$ temperature range. This is in a very good agreement with the 16.2 $J \cdot g_{ZIF-8}^{-1}$ experimental change of heat of intrusion over the same temperature range.

From semi-quantitative agreement between experimental and theoretical results, with the latter obtained using force fields designed for bulk systems without any tuning to consider the MOF/water interface, it is proposed that $\Delta\underline{C}_p$ is mostly due to confinement induced by ZIF-8 on water. Following from previous articles [12,13], the density of water confined within ZIF-8 cavities was much lower than the value of the bulk liquid, ~ 0.7 kg·dm^{-3}. As the specific heat capacity of bulk water decreases with increasing density, it is proposed that the effect of lowering the density below the bulk value at ambient pressure has the complementary effect of increasing the heat capacity.

This qualitative conclusion cannot be turned into a quantitative argument, as estimations of the heat capacity of bulk water at a ~ 0.7 kg·dm^{-3} are impossible: no experimental data are available for bulk water in these high tensile conditions. Neither experiments nor present simulations allow for the distinction between bulk-like and interface-like (between confined water and internal ZIF-8 surface) contributions to the heat capacity of confined water.

5.1.2 Effect of different non-wetting liquids on the heat of intrusion-extrusion. Evaluation of Concentration/Dilution Process on the Thermal Effect Using Non-intruding Solutes in Solution

We proposed a novel strategy for tuning heat of intrusion by exploiting the enthalpy of dilution as the aqueous solution concentrates upon the preferential intrusion of pure water into pores [1]. Reversed process affects the heat of extrusion.

With the water intrusion experiments verified, it was suspected that a heat of dilution effect could be present should the molecule be too large to enter the pore. So, the strategy turned to concentrated solutions with solutes that possess a significant and distinct heat of solution behaviour at various concentrations, and that would possess a bulk size large enough so that it would not pass through the nanopore opening. This strategy relied on the intrusion of only water into ZIF-8 from an aqueous solution, which then changes the concentration of the solution. Upon intrusion, concentration increases outside the porous system and diminishes to zero in the liquid inside the pores. A heat of dilution was then introduced into the energy balance associated with the intrusion-extrusion cycles. Two types of solutions were evaluated with respect to the heat of intrusion: aqueous solutions of potassium bromide [KBr] and of tert-butanol [Tert]. Both of these solutions have heat of solution values measured and reported in the literature, providing a direct way to evaluate the initial hypothesis and to exploit the heat of solution during the intrusion-extrusion cycle.

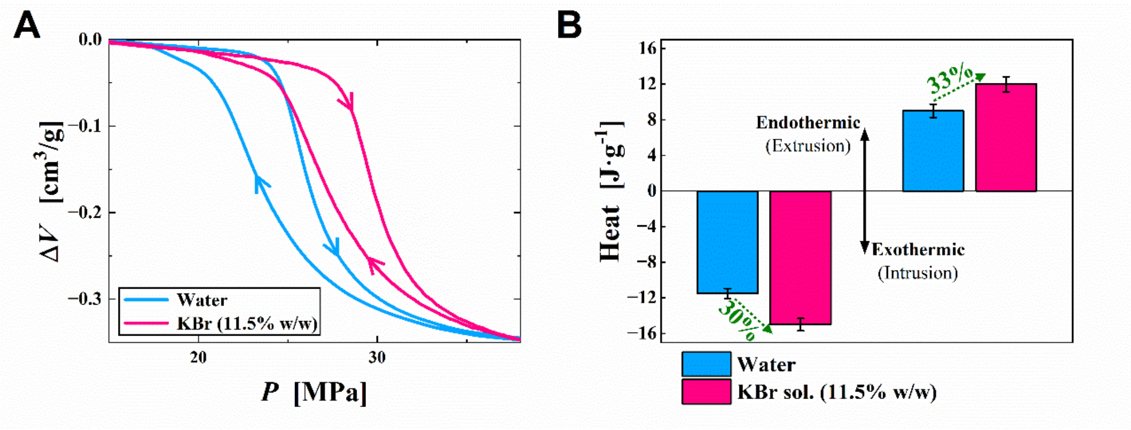

Figure 9.- Experiments at 298.15 K for mechanical intrusion-extrusion isotherms with the heat of intrusion and extrusion of water compared to the heat values of aqueous potassium bromide (11.5 w_t%)

The initial solution experiments provided insight into the heat generation process of concentration and dilution through the preferential intrusion of water into ZIF-8. The dissolution of KBr into water is endothermic in nature and decreases in thermal energy with increasing concentration. This means that the enthalpy of dilution is an endothermic phenomenon with the concentration phenomenon being exothermic as determined by the heat of solution data [14]. Figure 9 shows the experimental result from transitiometer experiments. For a solution of 11.5 w_t% KBr, the measured heat of intrusion was much larger compared to the theoretical estimate obtained by summing the heat of intrusion of pure water and heat of dilution. This was thought to be because the exclusion of KBr ions from the ZIF-8 pores is more complex than the heat of solution process. To further evaluate the strategy, we turned to MD simulations.

A simpler porous system than ZIF-8 was taken: a wide conical crevice, whose intrusion was barrierless and required no special simulation techniques to be studied [15,16], thus limiting the difficulties and allowing the study of the complex problem of heat of intrusion of a solution. We considered three cases: i) pure water, ii) KBr allowed to enter the crevice and iii) KBr prevented from entering the pore (see Figure 10).

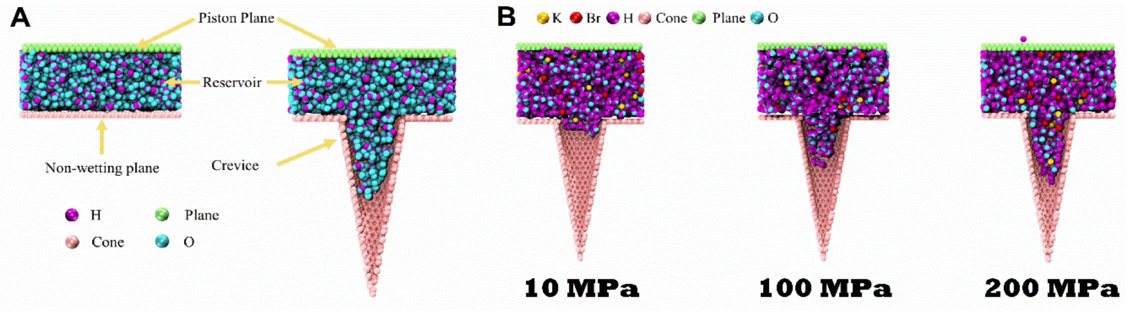

Figure 10.- Molecular dynamics of intrusion for the conical crevice. (A) Configurations to simulate intrusion where the first system consists of a liquid reservoir situated between two flat planes and the second system where a flat plane is transformed into a plane featuring a 2 nm diameter hole with a crevice (nano-cone). (B) Snapshots of the Visual Molecular Dynamics (VMD) for the intrusion of the KBr solution at 10, 100 and 200 MPa.

In all three cases, intrusion presented with the typical S-like profile of the curve of intruded water molecules *vs* pressure (Figure 11 A), like the typical experimental PV isotherms obtained experimentally. The number of water molecules entering the crevice upon pressure increase was very limited up to 30 MPa, after which a pronounced intrusion step was described up to 120 MPa, corresponding to the stage at which the intrusion transpired (Figure 11 B). At higher pressures, the system reaches a plateau up to 250 MPa, the maximum pressure explored the simulations.

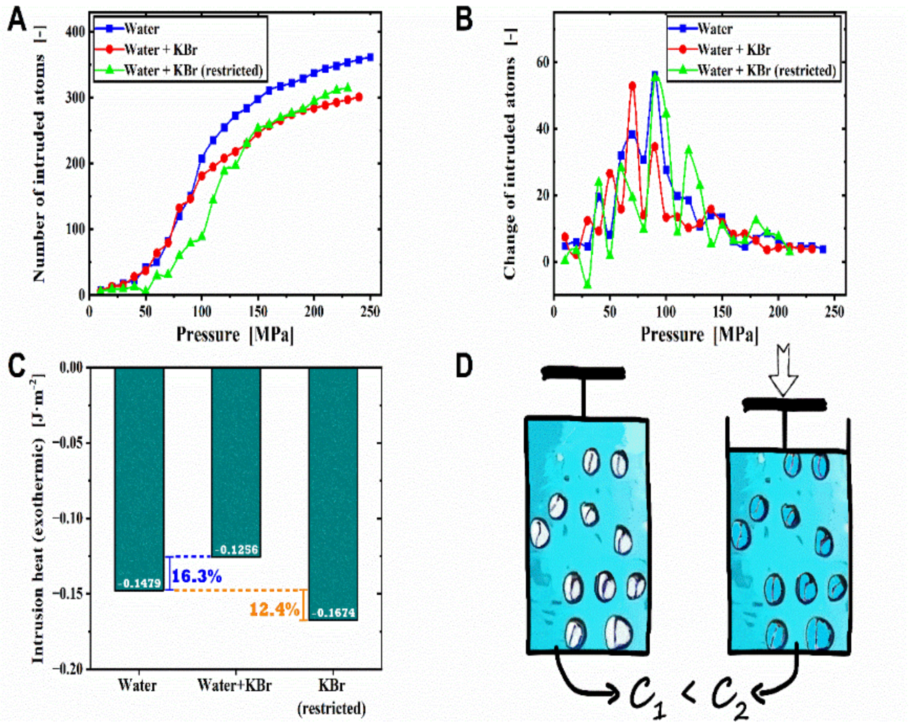

Figure 11.- Heat performance of the intrusion process by MD simulations. (A) The number of intruded atoms in the crevice relative to pressure for the three simulated systems: water, free-KBr and restricted-KBr atoms. (B) The change in the number of intruded atoms with respect to the previous pressure point depending on the pressure for the three simulated systems: water, free-KBr and restricted-KBr atoms. (C) The intrusion heat for the three simulated systems: water, free-KBr and restricted-KBr atoms. (D) Nano-pores acting as a filter to concentrate the solution components upon preferential water intrusion.

In the case of the solution where KBr was prevented from intruding, it was observed that there was a notable increase in intrusion pressure, ~20 MPa, which was qualitatively consistent with the ~5 MPa experimental shift. Conversely, when KBr was allowed to enter the crevice, no increase of the intrusion pressure was observed. This observation suggested that the increase in the intrusion pressure observed experimentally for the ZIF-8 and KBr solution was related to the preferential intrusion of water from the KBr solution. Similar shifts of intrusion pressure of salt solutions have been previously reported in the literature [17].

With respect to the heat effects, it was noticed that when KBr was allowed to enter the crevice, the process was less exothermic, while the opposite trend was observed when the salt was prevented from entering the cavity (Figure 11 C). This phenomenon is in line with the heat of concentration and dilution of salts in water, which is our macroscopic, thermodynamic explanation of the phenomenon. Experimentally, it was observed that the intrusion of the KBr solution into ZIF-8 was more exothermic, although the values were smaller than the predictions based on the solution enthalpy. This quantitative mismatch is attributed to a partial intrusion of the salt ions into the MOF, as reported in the literature results.

Considering the positive agreement between experiment and simulation, the possibility of endothermic intrusion into ZIF-8 was explored. Tert-butanol solutions were used, as it is a large and bulky non-intruding organic molecule and it possesses a heat of solution with large differences in heat over its miscible solubility range. From Figure 12, using aqueous solutions of 11.5 w_t% of tert-butanol demonstrated a small reduction in the theoretical exothermic heat of intrusion, whereas extrusion became less endothermic. Experimentally, a negligible change was observed for intrusion but extrusion was more significantly affected. This was expected in view of the heat of solution for water and tert-butanol from the published data by Koga [18]. When the concentration was raised to 32 w_t%, the heat of intrusion became endothermic while extrusion became exothermic. Similar results were observed for the 50 w_t% solution, with a greater amount of heat energy stored. In all cases, the heat of dilution calculations qualitatively supports the experimental outcome. The process of liquid intrusion-extrusion can thus be tuned by the preferential intrusion phenomenon when the solution enthalpy is dominant and defines the overall thermal effects of intrusion-extrusion.

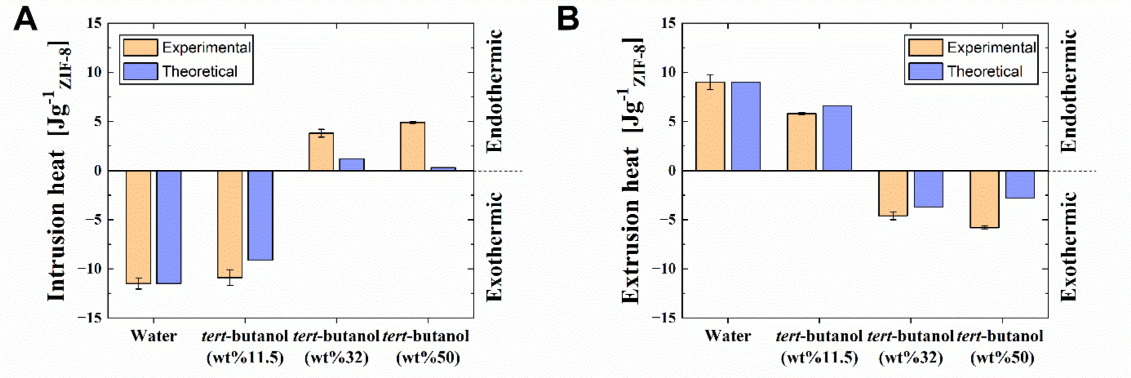

Figure 12.- A) Heat of intrusion of the different concentrations of aqueous tert-butanol solutions B) Heat of extrusion from the dilution of aqueous tert-butanol solution. The experimental values are shown in beige while the calculated difference between the heat of liquid water intrusion and concentration/dilution are shown in blue. All experiments were conducted at 298 K.

Further experiments were conducted to observe the effect of temperature on the heat of intrusion and extrusion. The temperature dependent experiments were continued with aqueous tert-butanol for this purpose, since the reported solution enthalpy becomes more endothermic with increasing temperature. Hypothetically, this would have the same effect on the heat of intrusion/extrusion. The results of individual experiments at higher temperature are shown in Figure 13. As the temperature increases, the heat of solution properties become more endothermic, resulting in lower absolute heat values. Thus, the solution properties have a reduced effect on the heat of intrusion and extrusion. This is observed for solutions of 32 w_t% and 50 w_t% above 40 °C where the heat of intrusion and extrusion are smaller than the heats at 25 °C. As the temperature decreases to 5 °C, the heat of intrusion and extrusion effects are larger than 25 °C due to the solution properties. From these experiments, it becomes apparent that solute choice is critical for augmenting or diminishing the heat of intrusion. At this point, there is not enough concentration-dependent heat of solution data for aqueous systems available to make an effective pairing for optimizing preferential intrusion.

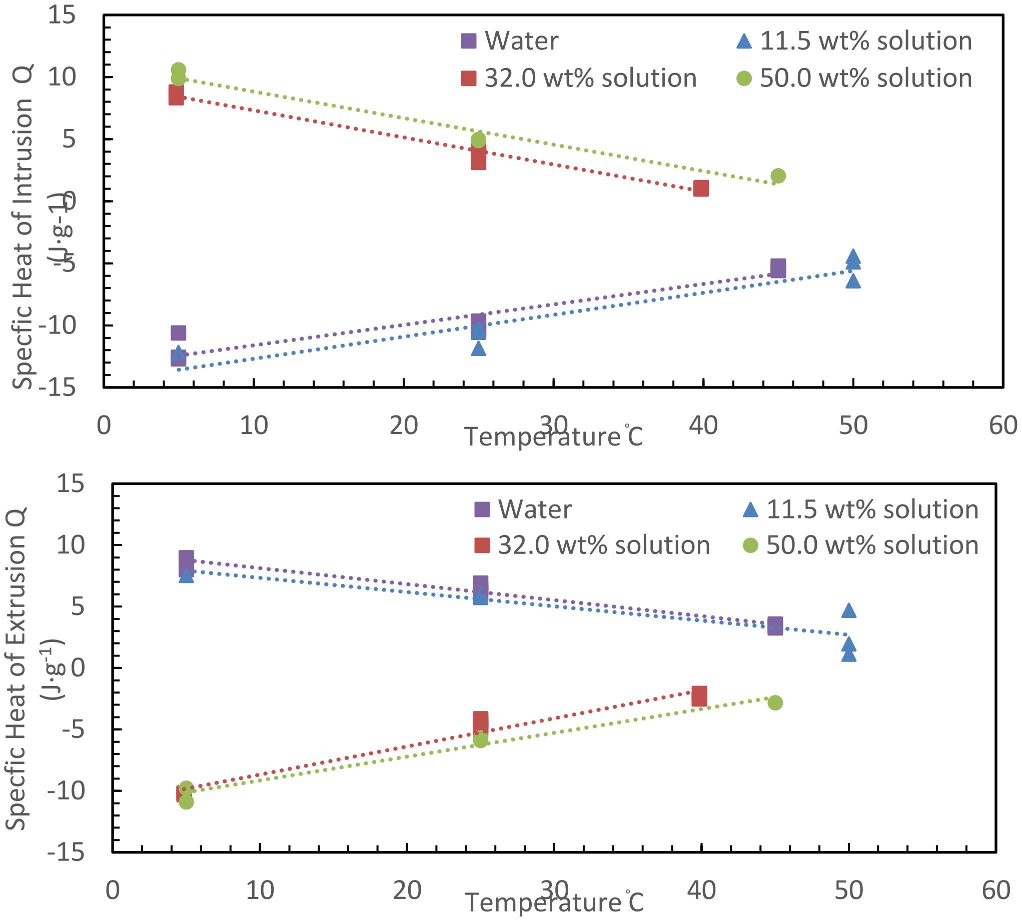

Figure 13.- Top figure is the heat of intrusion and bottom figure is heat of extrusion for aqueous tert-butanol solutions with respect to temperature and changing concentration. Each data point represents one calorimetric experiment

Tert-butanol Simulations

An MD investigation from ZIF-8 with different alcohols demonstrated that tert-butanol cannot enter into the cavities of ZIF-8. The investigation required the identification of suitable alcohols, specifically molecules which had a suitable size preventing their intrusion into ZIF-8, but whose solutions presented the smallest possible difference in viscosity to ensure that intrusion-extrusion was a relatively quick process. Methanol, ethanol, glycerol and tert-butanol were considered. The intrusion of tert-butanol into the ZIF-8 cavities (tert-butanol being a sample which presents convenient solution enthalpies) was predicted by our simulations to be energetically unfavourable (positive value of free energy, Figure 14 A). Based on these results, experiments were performed confirming that, in contrast with pure water, intrusion of tert-butanol solutions in ZIF-8 was endothermic.

Tert-butanol also presented a significant disadvantage. Its free energy as a function of the distance from the 6-membered ring apertures of ZIF-8 presented a minimum at a small distance from the MOF interface, corresponding to a high probability of finding these molecules at this interface (Fig. 1.2.3.2.15 B). This is due to the amphiphilic nature of tert-butanol, with both hydrophilic and hydrophobic groups. This resulted in a tert-butanol film physiosorbed to the ZIF-8/water interface, clogging the MOF apertures and inhibiting the intrusion-extrusion process.

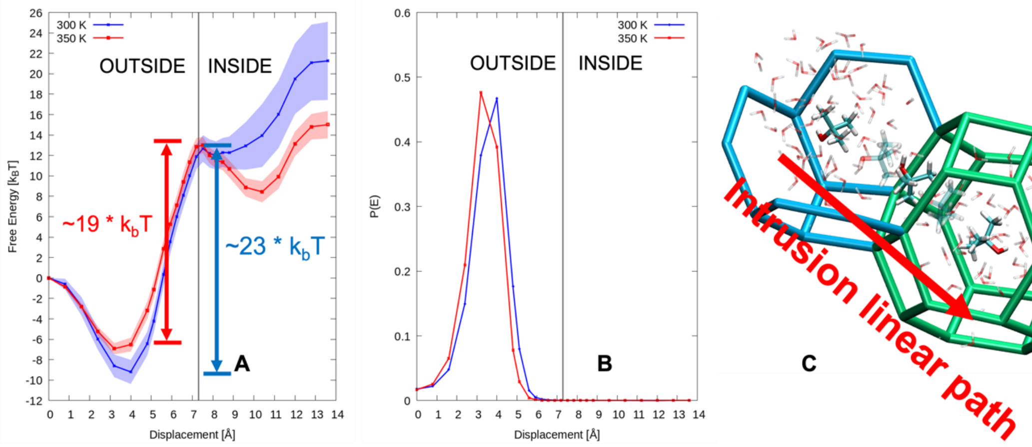

Figure 14.- Energetically unfavourable intrusion of tert-butanol molecules into ZIF-8 pores. (A) Free-energy profiles of intrusion at 300 K and 350 K. The vertical grey line is the reference for the transition from outside ZIF-8 to inside the first adjacent cage. (B) Probability to find the tert-butanol molecule along the intrusion path as the normalized exponential of the two free-energy profiles at 300 K and 350 K. (C) Illustrative example of the intrusion path perpendicular to the hexagonal window of ZIF-8.

The heat of solution can be exploited to manipulate the heat of intrusion-extrusion values. These findings were supported by a combination of thermodynamic literature and molecular dynamics simulations, which identified the effects of concentration and size exclusion that allowed for the intrusion of water into the pore cavities. Cumulatively, this highlights the gains and future challenges in identifying workable solutes and solutions.

5.1.3 Evaluation of the Particle Size/Flexibility on the Thermal Effects

In most recent investigations, the effect of the size of the ZIF-8 particles was explored. Micro particle-sized material was procured from commercial suppliers, whereas nanoparticles were synthesised as part of the WP2, and their synthesis procedures will not be discussed in this section. The objective is to determine the effect of size on both the mechanical and thermal properties. The motivation for this study is due to highly improved kinetics of electrification for nanoZIF-8 as reported in Deliverable 2.1.

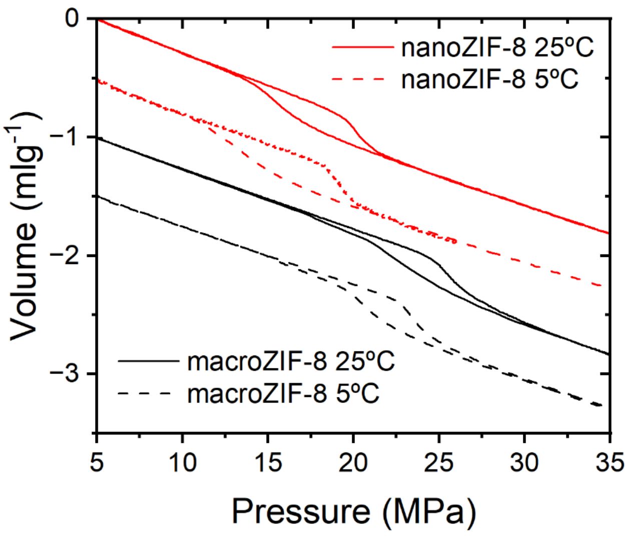

Figure 15.- Water intrusion-extrusion isotherms of nano-(red) and macroZIF-8 (black) at 5 ºC and 25 ºC, displaced at intervals of 0.5 ml·g^{-1} for clarity.

Table 1.- Average *P*, *V*, and *Q* values for NanoZIF-8 and MacroZIF-8

Isotherms	**V_{INT} (cm^{3}g^{-1})**	**V_{EXT} (cm^{3}g^{-1})**	**P_{INT} (MPa)**	**P_{EXT} (MPa)**	**Q_{INT} (Jg^{-1})**	**Q_{EXT} (Jg^{-1})**	**Temperature (K)**
NanoZIF-8	0.32	0.3	19.1	13.4	-9.7	7.0	278.15
NanoZIF-8	0.28	0.23	20.1	15.5	-7.0	4.8	298.15
MacroZIF-8	0.33	0.29	26.1	22.9	-12.0	9.4	298.15
MacroZIF-8	0.37	0.3	23.7	21.0	-14.8	10.5	278.15

PV-isotherms of two different ZIF-8 samples are shown in Figure 15, where macroZIF-8 refers to the commercial sample and nanoZIF-8 refers to the sample that was synthesized and characterised by CICe. The slope of all the curves is constant at low pressure, which is related to the compressibility of the system. When a certain pressure is reached, Pint, water begins to enter the porous material, giving rise to a sharp change in volume. NanoZIF-8's Pint appears at the lower pressure of 20.1 and 19.1 MPa while macroZIF-8's inflection point appears at 26.1 and 22.9 MPa at 298 K and 278 K, respectively. Returning to the initial slope of the curve is an indication of the filling of pores with water molecules. Upon the reduction of pressure from its maximum value, extrusion occurs. The behaviour of the complete intrusion and extrusion process is reproducible and resembles that of a shock absorber. In all cases, the absolute values of the intrusion-extrusion volume, pressure and heat are larger for the macroZIF-8 particles than the nanoZIF-8 particles. Their respective averages are given in Table 1.

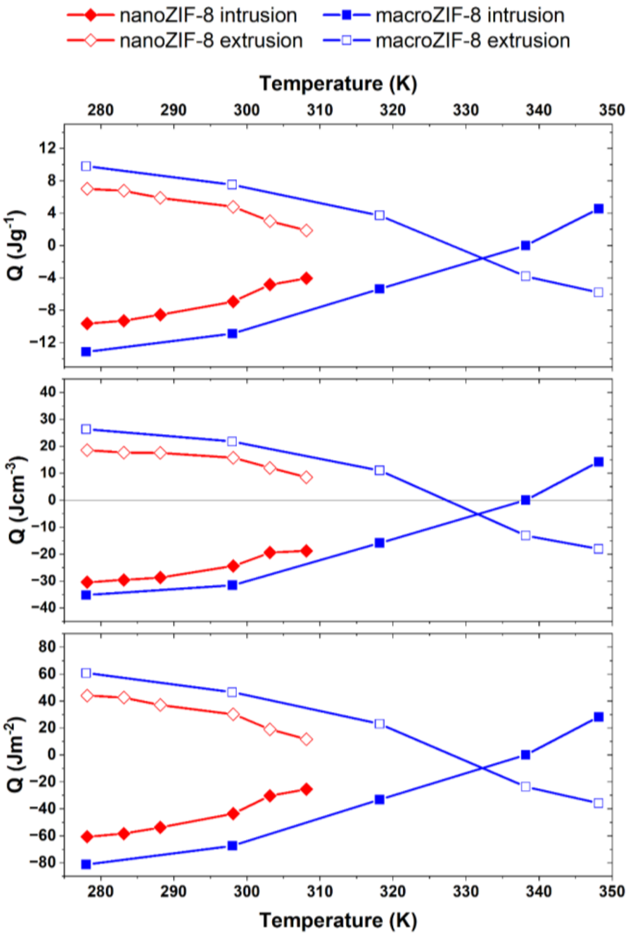

Figure 16.- a) The heat of intrusion/extrusion vs temperature of nano- and macroZIF-8, including the enthalpy sign inversion at higher temperatures for macroZIF-8; b) the heat of intrusion/extrusion accounting for differences in intrusion volume, and c) the heat of intrusion/extrusion accounting for differences in surface area.

The heat of intrusion/extrusion of nanoZIF-8 and macroZIF-8 with different temperatures are plotted in Figure 16. From 278 K to 308 K, both ZIF-8 samples exhibited exothermic intrusion and the measured heat of macroZIF-8 was larger than its nano counterpart. Temperature rise decreases exothermic tendencies of the systems. NanoZIF-8 was degraded at 310 K, and for this reason was not measured at higher temperatures. Intrusion of macroZIF-8 became endothermic after 340 K. Also, Figure 16. b), and c) depict the normalized heat values with respect to intrusion volume and surface area of the materials. The graphs in Figure 16. were similar, suggesting that the intrusion volume and surface area of the materials in isolation do not have deterministic effects on the magnitude and direction of the heat generated in the system during intrusion/extrusion.

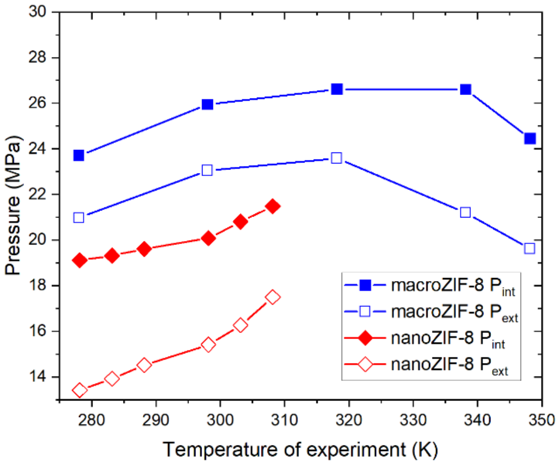

Figure 17.- Pint/ext of nanoZIF-8 and macroZIF-8 at different temperatures.

Figure 17 plots the intrusion/extrusion pressures (P_{int} and P_{ext}) as a function of the temperature of the experiments. In the case of nanoZIF-8, the stepwise rise in temperature up to 310 K resulted in a steady increase in P_{int} and P_{ext}. Further effects of temperature on pressure could not be recorded due to the instability of the material. Similarly, macroZIF-8 provided a slight increase in the P_{int} and P_{ext} values within the same temperature range. Further increasing temperature resulted in pressure values reached a maximum point and then decreased with further increases in temperature.

The computation of size effects

The reduction of particle size down to the nanoscale led to a reduction in intrusion pressure of ZIF-8. Considering the temperature is equal to 300 K as a reference, the P_{int} drops from 25 to 20 MPa, as reported in Johnson *et al.* 2023 [13]. Experimental data mentioned above show that the reduction of P_{int} is associated with a reduction of intrusion heat of 30 %, with the process becoming less exothermic.

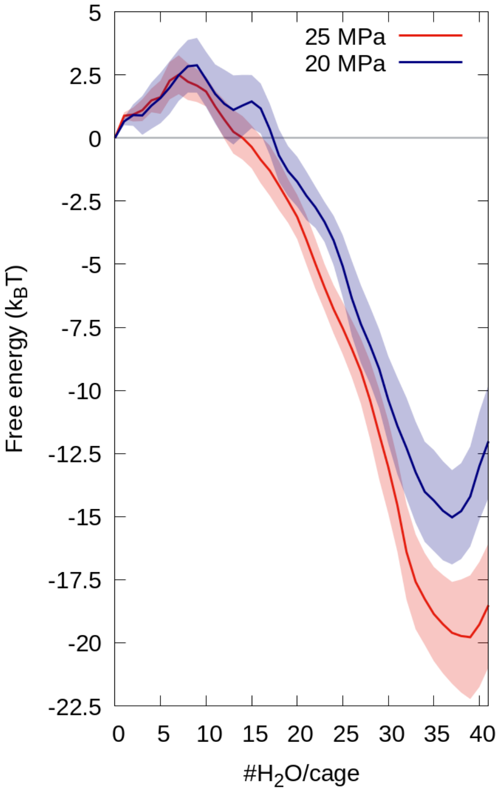

Figure 18.- Free energy of filling, expressed in kBT, against the number of water molecules inside a ZIF-8 cage at 20 (blue) and 25 MPa (red). Reducing the pressure, the energy of the stable-state was reduced by ~5 k_BT. The minimum is also reached with fewer water molecules, from 39 (at 25 MPa) to 37 (at 20 MPa) molecules per cage.

From a previous analysis of the free energy of filling a single ZIF-8 cage [19], a reduction in P_{int} was accompanied by a reduction of the number of water molecules intruded into the cage. Simulations were performed at 300 K with a 2x2x2 ZIF-8 supercell that consisted of 16 cavities. They were filled with 632 or 592 water molecules for the samples subjected to 25 MPa (corresponding to the standard intrusion pressure of ZIF-8) and 20 MPa (P_{int} of nanoZIF-8), respectively. The result of the change in intrusion heat between macroZIF-8 and nanoZIF-8 samples was calculated to be 33 %, in agreement with the experimental data. Smaller cage values are represented in Figure 18.

With this result, the conditions of the simulation were altered to observe whether this change was related to the reduction of P_{int} in macroZIF-8 or was related to the reduction of water molecules intruded into the system. To see the effect of pressure, the system was filled with 632 water molecules at 20 MPa (the same filling level but at a lower pressure). Under these conditions, the heat reduction was only 3 %. Simulating the system with 592 water molecules at 25 MPa (the lower filling level at the same pressure) yielded a reduction of heat of 26.4 %.

In summary, we found that the decrease in intrusion heat comes from two main factors: a drop in intrusion pressure and a decrease in the amount of water that enters. Our calculations showed that the reduction in water molecules entering plays a much bigger role than the change in intrusion pressure.

6 HEAT OF INTRUSION/EXTRUSION INTO FROM SILICA BASED SYSTEMS

As part of WP2, hydrophobic porous silicas were synthesised. The silica particle surface was modified by perfluorosilane moieties to produce CF3-Silica. The obtained calorimetric results of CF3-Silica are shown in Figure 19.

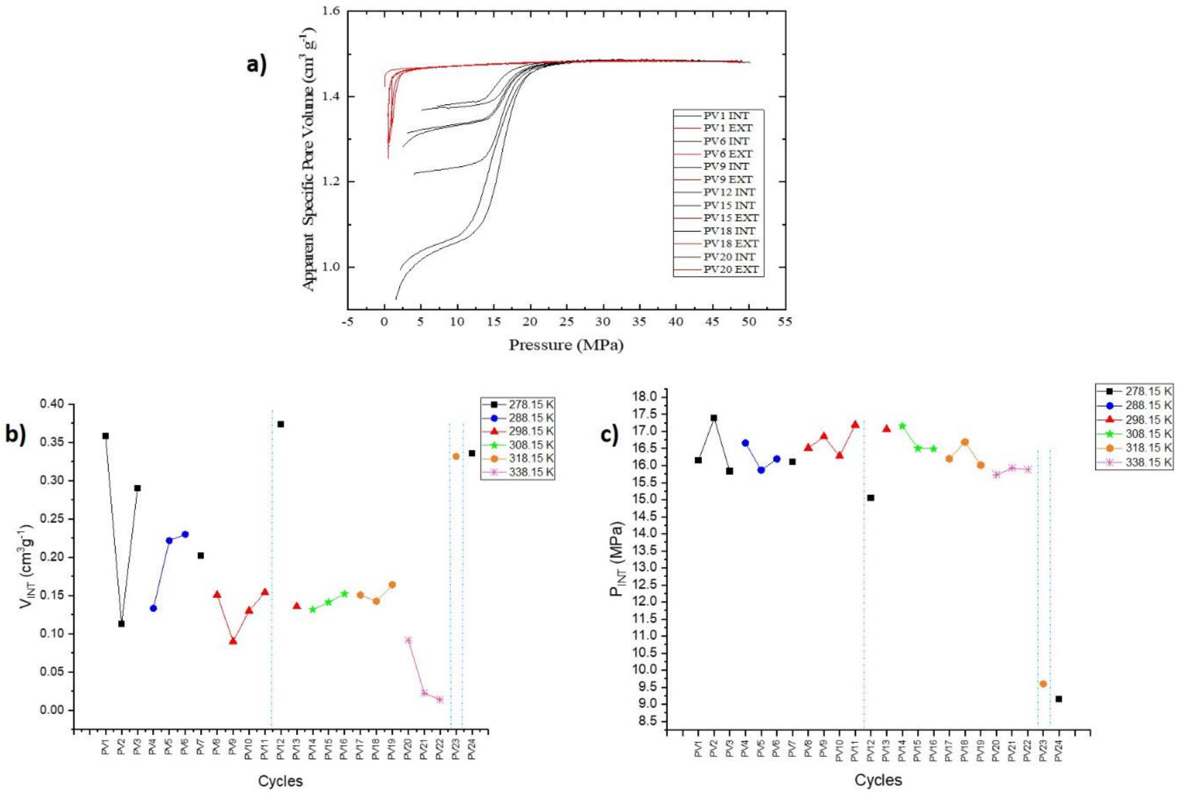

Figure 19.- Specific Volume of Intrusion and Intrusion Pressure into CF3-Silica and water by transitiometry with respect to each cycle.

The experimental results indicated that sequential PV cycles, where the silica was completely reversible, were not possible, and extrusion properties were not recorded. A possible reason for this behaviour could be the time taken to complete a compression and decompression cycle in the transitiometer. To understand whether the sample decomposed after consecutive PV cycles, the CF3-Silica samples were removed from the calorimeter cells and dried overnight under a vacuum at 50 °C. This procedure was implemented specifically after PV cycles 11, 22, and 23 (indicated with dashed blue lines in Figure 19 (b,c). Drying the sample regenerated the CF3-Silica, but regeneration trials were unsuccessful after exposing the material to higher temperature experiments at 338 K. During the intrusion process, all the heat values were exothermic, Figure 20, but no heat effects were observed for extrusion.

This provides important operational information for the prototype (avoiding long compression pauses required) and on the stability of the material at higher temperatures.

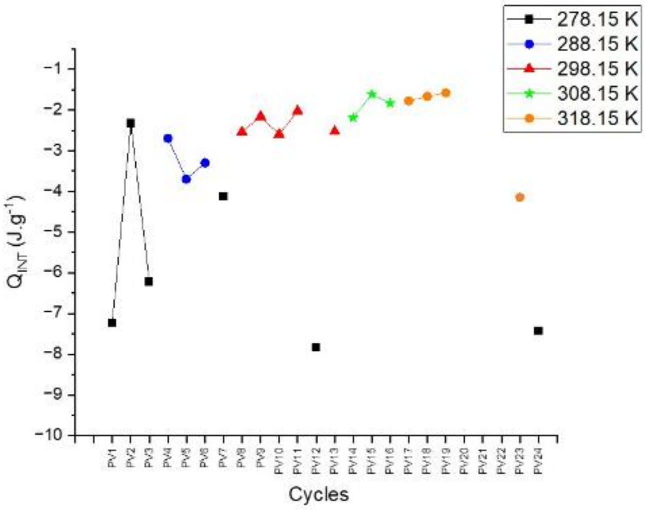

Figure 20.- Specific Heat of Intrusion results for CF3-Silica sample and water by transitiometry with increasing temperature and respect to each cycle.

Considering the meso-size pores, we attempted to introduce solid conductive particles into the intrusion-extrusion process to try increasing the charge transfer. C60 fullerene nanoparticles were chosen, as they demonstrated the ability to enhance the electrification effects during intrusion-extrusion, but thermal effects had not yet been studied for this purpose. Further research with a fresh sample of CF3-Silica was carried out by altering the intruding liquid phase from water to nanofluid, so-called "Polyethyleneimine modified C60", whose structure is depicted in Figure 21 (C60-PEI hydrochloride, 1 mg·ml^{-1} that is equal to 7.6 x 10^{-4} M and pH 2.6 HCl Solution).

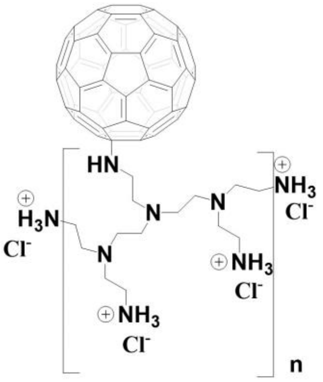

C_{60}PEI (hydrochloride)

Figure 21.- Structure of used nanofluid instead of water.

Presented in Figure 22 is the result of the experiments using nanofluids as the intruding liquid. In contrast to earlier results, measured V_{int} values were more consistent with cycling than the previous sample. It was found that the application of Nano fluid provided a benefit in terms of adequate spontaneous extrusion of the liquid and eliminated vacuum drying of silica powder.

Comparison of the Q_{INT} value of water-based experiments (-2.4 ± 1 J·g^{-1}) and the nanofluid experiment (-5.6 ± 1 J·g-1), at 298.15 K, showed that Nanofluid resulted in a more than twofold increase of the heat. Above 378.15 K, no Qint/ext data was detected due to the possible structural degradation of CF3-Silica. As in the case of water, all Q_{int} values of Nanofluid trials are exothermic until 358.15 K. At this temperature, Q_{int} is zero and at the higher temperature of 378.15 K, the heat effects become endothermic.

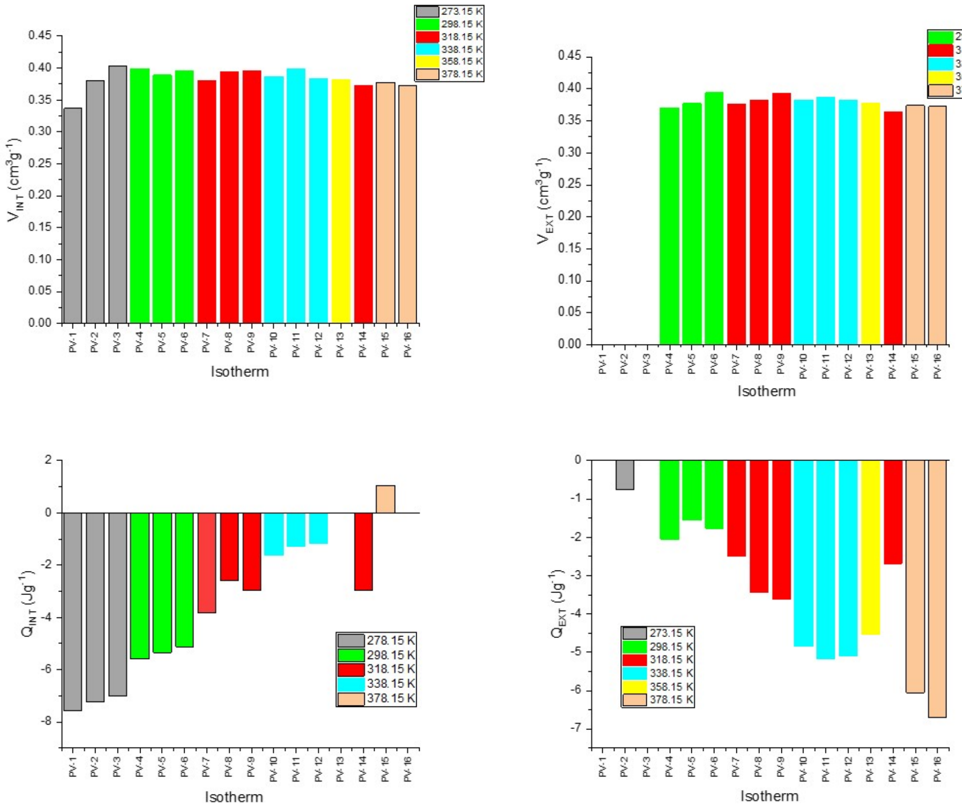

Figure 22.- Specific Volume of intrusion/extrusion ($V_{INT}/_{EXT}$) and Specific heat of intrusion/extrusion ($Q_{INT}/_{EXT}$) results of CF3-Silica and Nanofluid solution in the Scanning Transitiometry.

Further experiments have been carried out with commercially available silica gel (SymmetryPrep C8 (WC-8), (supplier: WATERS)). It differs from the CF3-Silica sample synthesized in WP2, as the hydrophobic properties of WC-8 are provided by grafting with silane bearing a hydrocarbon group. The results of the intrusion-extrusion experiments of water into WC-8 are plotted and compared with water/CF3-Silica and Nanofluid/CF3-Silica in Figure 23. The nanofluid/CF3-Silica and water/WC-8, heat of intrusion results are similar, with the differences between the two heat values being largest about the temperature of 378 K – 382 K. The largest differences are in the heat of extrusion values, where the heat of extrusion of WC-8 is much greater (3.6 J·g^{-1}) than that of the Nanofluid/CF3-Silica.

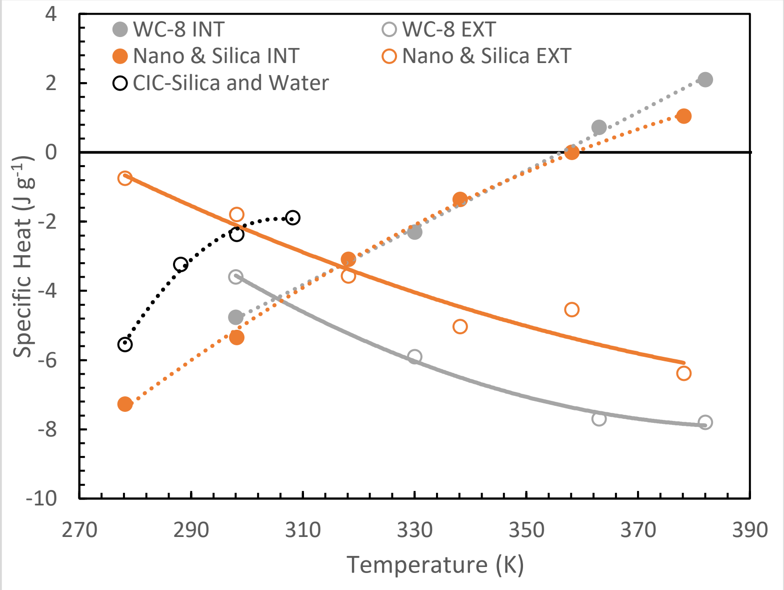

Figure 23.- $Q_{INT/EXT}$ results of CF_3-Silica with water and CF_3-Silica with Nanofluid WC-8 with water from the scanning transitiometer.

Simulation of Grafted Silica

Simulations were conducted in parallel on a model mimicking WC-8, consisting of a silica slab grafted with the same hydrocarbon used in WC-8 experimental samples. It was necessary to resort to this planar system because WC-8 pores have a characteristic size of several tens of nanometers. Considering the number of water molecules necessary to fill them, the calculations would be prohibitively computationally expensive and the model would not be useful at the curvature of the material, as this is not expected to play a crucial role for such large pores.

Considering the positive validation of the Kelvin-Laplace formula for ZIF-8, we applied the same approach for computing the heat of intrusion in the model WC8, which requires estimating the value of the contact angle of the solid and its temperature dependence. In Figure 24, we report the contact angle vs T trend. In contrast with ZIF-8, the trend is not monotonic.

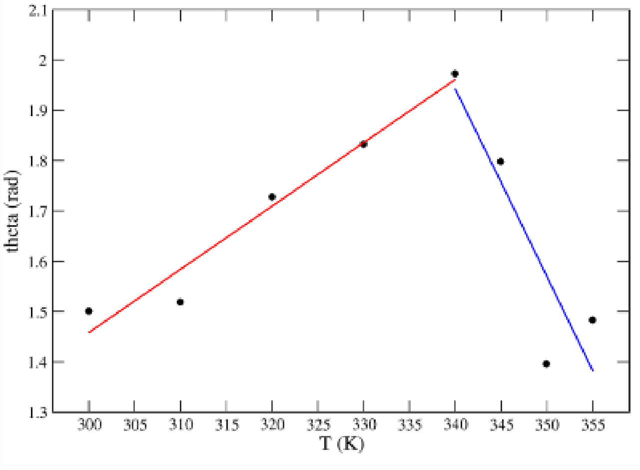

Figure 24.- WC-8 contact angle at different temperatures.

The contact angle first increases and then decreases with T. This brings a change from negative to positive heat of intrusion for temperatures below and above ~340 K (Figure 25). Once again, this trend is in qualitative agreement with experimental results, though from the quantitative point of view the absolute value of the theoretical heat of intrusion is much larger than the experimental data, as it was for ZIF-8. We believe that processes that cannot be modelled by classical molecular dynamics take place together with intrusion, which may be responsible for the quantitative difference. Identifying these mechanisms is one of the main objectives of the final period of the project.

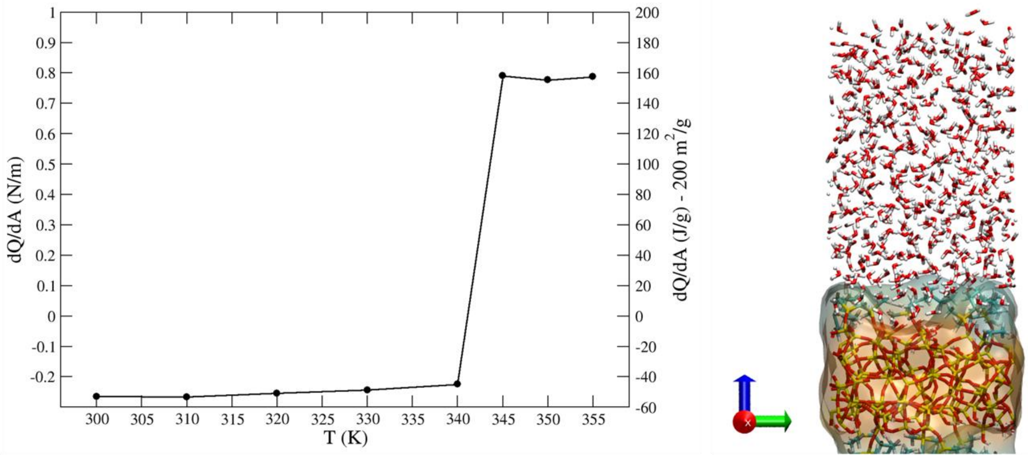

Figure 25.- (Left) Heat of intrusion of CH3-Silica sample calculated at different T applying Kelvin-Laplace equation (Right). Computational sample of the grafted silica surface in contact with bulk water molecules.

7 An Alternative Direction to Tune the Heat of Intrusion by using D_2O with ZIF-8.

Figure 26 shows the PV isotherms of heavy water (solid lines) and light water (dashed lines) moving into (shown with black lines) and from (shown with red lines) the pores. It can be seen that there is a distinct difference between the intrusion and extrusion pressure of each of these intruding liquids. The intrusion/extrusion pressure of heavy water is greater than that of light water.

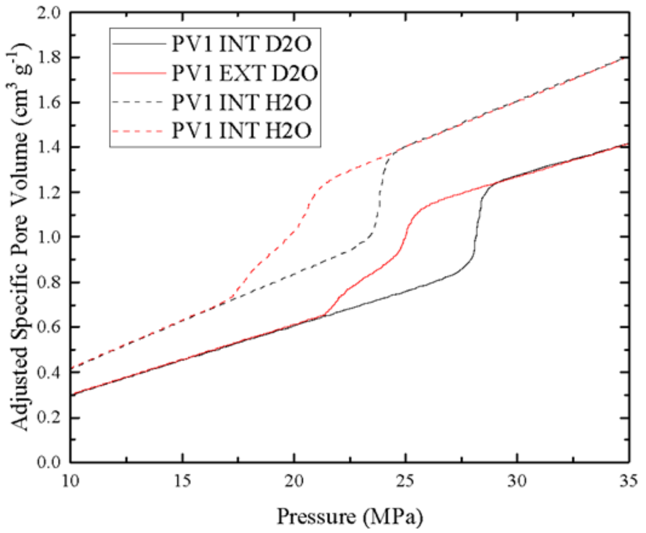

Figure 26.- PV isotherm of outgassed ZIF-8 filled with water (dashed lines) and heavy water (solid lines).

From high-pressure calorimetry experiments, the specific pore volumes were calculated and compared to each other. At 278 K, the specific pore volume for light water is 0.379 $cm^3 \cdot g^{-1}$ vs 0.380 $cm^3 \cdot g^{-1}$ for heavy water, with the standard deviation being ± 0.01 $cm^3 \cdot g^{-1}$. The temperature dependence of the mechanical properties of specific pore volume and intrusion/extrusion pressure are depicted in the Figure 27 and Figure 28. The differences between them become apparent with intrusion/extrusion pore volumes in Figure 27 decreasing with each successive cycle up to 338 K.

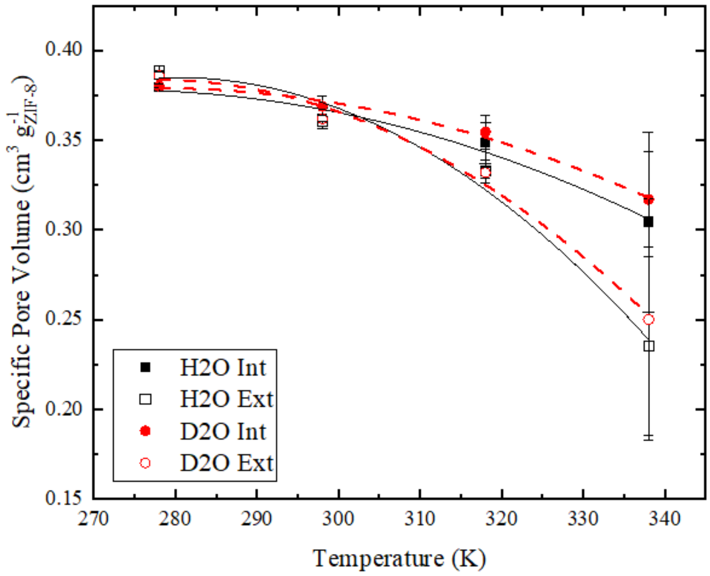

Figure 27.- Average intrusion/extrusion specific pore volumes of ZIF-8 with water and heavy water. The lines are visual guides for the eye.

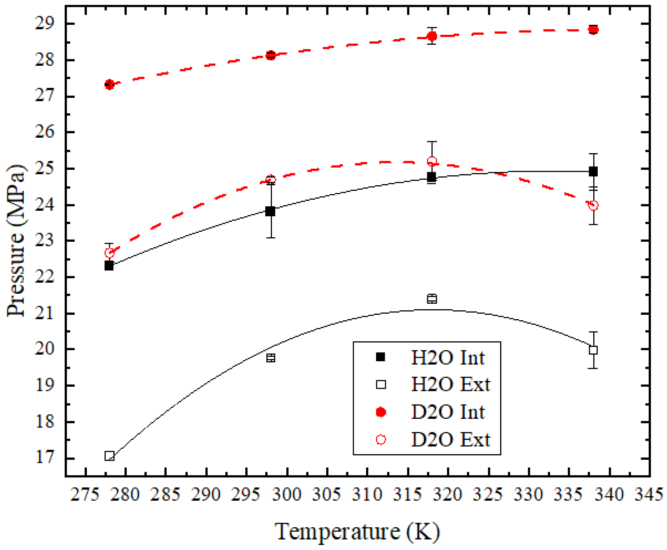

Figure 28.- Average Intrusion and Extrusion Pressures of light and heavy water moving into/from ZIF-8 with increasing temperature. The lines are visual guides for the eye.

At 338 K, the specific pore volume values decrease with each cycle until intrusion/extrusion cycling is no longer possible. For both experiments, intrusion and extrusion pressures, as seen in Figure 1.2.3.128 B, are consistently larger in D_2O than in H_2O, and follow similar temperature-dependent patterns. During the intrusion process, the temperature curve follows a weak parabolic shape to the intrusion pressure values. The extrusion curve shows a more distinct parabolic trend with temperature.

The intrusion pressure is described by the Young-Laplace equation $P_{int}= \gamma \cdot \cos(\vartheta) r^{-1}$ where γ is the surface tension, ϑ is the interfacial contact angle, and r is the pore radius. The variable r is constant and ϑ cannot be adequately described at the nanoscale, which leaves the surface tension for each of the liquids as the point of comparison. The surface tension of heavy water (γ = 71.8 $mJ \cdot m^{-2}$) [20] is lower than that of light water (γ = 71.96 $mJ \cdot m^{-2}$) [21], but the intrusion and extrusion pressures of heavy water are ~5 MPa greater than those of light water.

Similar to the intrusion/extrusion pressure, there is a significant difference between the heat of intrusion and the extrusion of light water and heavy water, as shown in Figure 29.

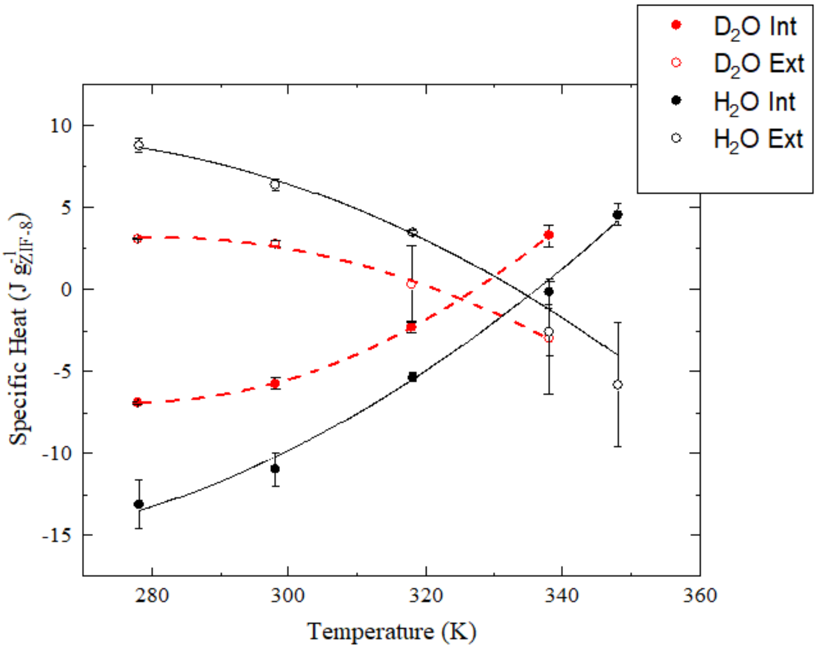

Figure 29.- Heat of intrusion and extrusion for both light and heavy water measured with and without atmospheric gases. The presented curves are a visual guide only.

Starting with the heat of the intrusion process, the difference between the respective thermal effects is 6 $J\cdot g^{-1}_{ZIF-8}$ at 278 K, while at a temperature of 338.15 K, the difference is reduced to 3 $J\cdot g^{-1}_{ZIF-8}$. The isotope effect shifts the heat in an endothermic direction. During the extrusion process, the heat follows a similar trend, where at 278 K the difference is at 5 $J\cdot g^{-1}_{ZIF-8}$ and 3 $J\cdot g^{-1}_{ZIF-8}$ at 318.15 K, in the exothermic direction. At the temperature of 338.15 K, the difference between light water and heavy water is 0.3 $J\cdot g^{-1}_{ZIF-8}$.

The thermal sign intercession point moves from approximately 335 K (light water) to 325 K (heavy water). This shift in thermal effects is significant and in line with other heat-related effects, including specific heat capacity, melting enthalpy, and the thermal expansion coefficients of heavy water [20], which possess lower values than light water. Consequently, the thermal effect is represented by the temperature-dependent surface properties known as the surface entropy ($d\gamma\cdot\cos\vartheta/dT$). In this case, the surface entropy of heavy water (-0.24 $mJ\cdot m^{-2}\cdot K^{-1}$) is greater than light water (-0.237 $mJ\cdot m^{-2}\cdot K^{-1}$) [21], but the thermal effect shows a significant change of heat with respect to the 0.008 $mJ\cdot m^{-2}\cdot K^{-1}$ difference in the surface entropy. Therefore, this trend is not supported by these macroscopic equations and may suggest a genuinely nanoscale effect. It does provide a route for adjusting the heat of intrusion/extrusion. In addition, this asks further questions about the nature of the process of intrusion/extrusion at the nanoscale.

8 CONCLUSIONS

The object of this deliverable is to achieve the "*optimal properties of porous materials and non-wetting liquids for heat of intrusion-extrusion maximization*". For this work package a great cumulative effort was made by partners across the consortium to create new materials, measure the heats of intrusion and extrusion and form a fundamental understanding of the heat processes.

We have found that heat effects depend on the structure, geometry, and topology of porous matrixes, the grafting protocol of mesoporous silica, the size of porous particles, temperature, and the chemical composition of liquids. We demonstrated how the hydrogen/deuteriumisotopic substitution affects intrusion-extrusion pressures and accompanied heat. To understand the phenomena at an atomistic level, intensive computer simulations were performed. They show qualitative and sometimes even quantitative correspondence with experiments. The main conclusions are:

1. Non-penetrating in porous matrixes organic compounds change the sign of heat effects (from ca. -10 to +10 J/g for water - tert-butanol mixtures and ZIF-8) depending on their concentration in an aqueous solution.
2. Temperature affects both intrusion-extrusion pressure and heat effects, thus, they may change a sing.
3. Inorganic salt aqueous solutions increase the absolute values of heat effects.
4. Isotopic effects demonstrated the role of hydrogen bond strength in intrusion-extrusion. Heavy water intrusion-extrusion demonstrates less pronounced heat effects.
5. With decreasing particle sizes, decrease the intrusion-extrusion pressure and heat effects.

Thus, these results show the path to design systems with specific properties. To maximize heat effects, one should use aqueous solutions at a narrow temperature range. For the design of systems without thermal effects aqueous solutions of the specific concentration is recommended. Experimentally observed heat effects were about 10-20 J/g.

From this combine effort we can distil our optimization strategy into two routes:

1) Temperature has the greatest impact on the heat of intrusion/extrusion, as it allows us to provoke endothermic intrusion at elevated operating temperatures. The range of temperature explored encompasses the operating temperatures of the shock absorber in real-world conditions.

2) The heat of intrusion/extrusion can be manipulated by using different solutes in water to exploit the heat of solution. We identified that, depending on the solutes, we can increase the total amount of heat from intrusion or even change the sign from exothermic to endothermic.

BIBLIOGRAPHY

1. Luis Bartolomé, Argyrios Anagnostopoulos, Alexander R. Lowe, Piotr Ślęczkowski, Eder Amayuelas, Andrea Le Donne, Michał Wasiak, Mirosław Chorązewski, Simone Meloni, and Yaroslav Grosu. Tuning Wetting−Dewetting Thermomechanical Energy for Hydrophobic Nanopores via Preferential Intrusion, J. Phys. Chem. Lett., 15, 4, 880–887 (2024).
2. Grosu, Y.; Renaudin, G.; Eroshenko, V.; Nedelec, J.-M.; Grolier, J.-P. E. Synergetic Effect of Temperature and Pressure on Energetic and Structural Characteristics of {ZIF-8+water} Molecular Spring. Nanoscale, 7, 8803– 8810, (2015).
3. Coiffard, L.; Eroshenko, V.; Grolier, J.-P. E. Thermomechanics of the Variation of Interfaces in Heterogeneous Lyophobic Systems. AIChE J., 51, 1246– 1257, (2005).
4. Karbowiak, T.; Weber, G.; Bellat, J.-P. Confinement of Water in Hydrophobic Nanopores: Effect of the Geometry on the Energy of Intrusion. Langmuir, 30, 213– 219, (2014).
5. Grosu, Y.; Li, M.; Peng, Y.-L.; Luo, D.; Li, D.; Faik, A.; Nedelec, J.-M.; Grolier, J.-P. A Highly Stable Nonhysteretic {Cu-2(Tebpz) MOF + Water} Molecular Spring. ChemPhysChem, 17, 3359– 3364, (2016).
6. Alexander R. Lowe, Piotr Ślęczkowski, Emre Arkan, Andrea Le Donne, Luis Bartolomé, Eder Amayuelas, Paweł Zajdel, Mirosław Chorążewski, Simone Meloni, and Yaroslav Grosu, Exploring the Heat of Water Intrusion into a Metal–Organic Framework by Experiment and Simulation. ACS Appl. Mater. Interfaces, 16, 4, 5286–5293 (2024).
7. A. Laouir, L. Luo, D. Tondeur, T. Cachot, P. Le Goff. Thermal Machines Based on Surface Energy of Wetting: Thermodynamic Analysis, AlChE J., 49, 764-781 (2003).
8. L. Maragliano, E. Vanden-Eijnden. A temperature accelerated method for sampling free energy and determining reaction pathways in rare events simulations, Chem. Phys. Lett., 426, 168-175 (2006).
9. J.B. Abrams, M.E. Tuckerman. Efficient and Direct Generation of Multidimensional Free Energy Surfaces via Adiabatic Dynamics without Coordinate Transformations, J. Phys. Chem. B, 112, 49, 15742–15757 (2008).
10. C. Caddeo, D. Marongiu, S. Meloni, A. Filippetti, F. Quochi, M. Saba, A. Mattoni. Hydrophilicity and Water Contact Angle on Methylammonium Lead Iodide, Adv. Mater. Interfaces, 6, 1801173, (2018).
11. D. Chandler. Introduction to Modern Statistical Mechanics, (Oxford U. Press, New York, 1987), 274 pages.
12. M. Tortora, P. Zajdel, A.R. Lowe, M. Chorążewski, J.B. Leão, G.V. Jensen, M. Bleuel, A. Giacomello, C.M. Casciola, S. Meloni, Y. Grosu. Giant Negative Compressibility by Liquid Intrusion into Superhydrophobic Flexible Nanoporous Frameworks, Nano Lett., 21, 7, 2848–2853 (2021).

13. L.J.W. Johnson, G. Paulo, L. Bartolomé, E. Amayuelas, A. Gubbiotti, D. Mirani, A. Le Donne, G.A. López, G. Grancini, P. Zajdel, S. Meloni, A. Giacomello, Y. Grosu. Optimization of the wetting-drying characteristics of hydrophobic metal organic frameworks via crystallite size: The role of hydrogen bonding between intruded and bulk liquid, J. Coll. Int. Sci., 645, 775–783 (2023).
14. Wüst, J.; Lange, E. Lösungs- Und Verdünnungswärmen von Salzen von Der Äussersten Verdünnung Bis Zur Sättigung. I. Z. Phys. Chem. 1925, 116U (1), 161–214.
15. A. Giacomello, M. Chinappi, S. Meloni, C.M. Casciola. Geometry as a Catalyst: How Vapor Cavities Nucleate from Defects, Langmuir, 29, 14873-14884 (2013).
16. A. Giacomello, C.M. Casciola, Y. Grosu, S. Meloni. Liquid intrusion in and extrusion from non-wettable nanopores for technological applications, Eur. Phys. J. B, 94, 163 (2021).
17. G. Fraux, A. Boutin, A.H. Fuchs, F.-X. Coudert. Structure, Dynamics, and Thermodynamics of Intruded Electrolytes in ZIF-8, J. Phys. Chem. C, 123, 25, 15589–15598 (2019).
18. Koga, Y. Excess Partial Molar Enthalpies of Water in Water– Tert -Butanol Mixtures. Can. J. Chem., 66 (12), 3171–3175 (1988).
19. Liam J. W. Johnson, Diego Mirani, Andrea Le Donne, Luis Bartolomé, Eder Amayuelas, Gabriel A. López, Giulia Grancini, Marcus Carter, Andrey A. Yakovenko, Benjamin A. Trump, Simone Meloni, Paweł Zajdel, and Yaroslav Grosu, Effect of Crystallite Size on the Flexibility and Negative Compressibility of Hydrophobic Metal–Organic Frameworks, Nano Lett., 23, 10682−10686 (2023).
20. IAPWS Release on Surface Tension of Heavy Water Substance, (September 1994), (http://www.iapws.org/relguide/surfd2o.pdf).
21. The International Association for the Properties of Water and Steam, (June 2014), (http://www.iapws.org/relguide/Surf-H2O-2014.pdf).

European Innovation Council

Funded by the European Union